Direct numerical simulation of turbulent condensation in clouds

By R. Paoli AND K. Shariff †

1. Motivation and objectives

Clouds are responsible for precipitation, scattering and absorption of electromagnetic energy, and cloud particles serve as sites for chemical reactions. To properly incorporate these processes in cloud-resolving codes or climate models, the crucial quantity required is the droplet size spectrum $n(r)$ within a computational cell, defined such that $n\,dr$ gives the number of particles in the cell having radii between r and $r + dr$. The role of turbulence in clouds has been the object of intensive investigation in the atmospheric science community over the last forty years. (Consult the reviews by Pinsky & Khain 1997, Vaillancourt & Yau 2000, and Shaw 2003). Turbulence has three effects on the development of the droplet size spectrum: (i) During the initial phase of condensational growth it causes each particle to experience a different fluctuating supersaturation as it is transported and this leads to a broadening of the spectrum (Cooper 1989). (ii) Turbulence causes particles to cluster when they become large enough that particle inertia becomes important; this clustering eventually influences the size spectrum during the coagulation phase. (iii) Finally, during the coagulation phase, turbulence increases the number of particle encounters. The present work aims to further elucidate the first of these effects with a view to developing sub-grid models for it. In the atmospheric sciences literature, this effect is referred to as "stochastic condensation."

The first step in current approaches for modeling stochastic condensation (see for example Khvorostyanov & Curry 1999*a*) is to write down the transport equation,

$$\frac{\partial f}{\partial t} + \frac{(\partial f u_j)}{\partial x_j} = \frac{\partial (f\,\dot{r})}{\partial r}, \tag{1.1}$$

for the particle size distribution $f(\mathbf{x}, r, t)$. Here $f(\mathbf{x}, r, t)d\mathbf{x}\,dr$ gives the number of particles in the four dimensional phase space volume $d\mathbf{x}\,dr$ at $(\mathbf{x}, r)$. The next step follows the standard approach for Reynolds averaging. Decomposing variables into mean and fluctuating parts, $f = \overline{f} + f'$, $r = \overline{r} + r'$, and averaging the entire equation leads to the appearance of covariances like $\overline{u_j' f'}$ or $\overline{\dot{r}' f'}$ which are modeled using a mixing length approach. Khvorostyanov & Curry (1999*b*) were able to obtain a solution for $\overline{f}$ in terms of gamma functions which is an attractive result as many observed cloud-droplet distribution can be fitted with gamma distributions (Shaw 2003). One of the assumptions made by those authors was to use a linear relation between droplet growth rate and supersaturation fluctuations, $\dot{r}' \sim S'$, based on the analysis by Srivastava (1989) and heuristic considerations about the equivalence between Brownian motion of small particles and the motion of turbulent eddies.

In this brief, we investigate the turbulent condensation of a population of droplets by means of direct numerical simulation. To that end, a coupled Navier-Stokes/Lagrangian

† NASA Ames Research Center, Moffett Field, CA 94035

solver is used (see Paoli *et al.* 2004) where each particle is tracked and its growth by water vapor condensation is monitored exactly. The main goals of the study are to find out whether turbulence broadens the droplet size distribution, as observed in *in situ* measurements. The second issue is to understand if and for how long a correlation between the droplet radius and the local supersaturation exists for the purpose of modeling subgrid scale microphysics in cloud-resolving codes.

This brief is organized as follows. In Sec. 2 the governing equations are presented, including the droplet condensation model. The implementation of the forcing procedure is described in Sec. 3. The simulation results are presented in Sec. 4 together with a sketch of a simple stochastic model for turbulent condensation. Conclusions and the main outcomes of the study are given in Sec. 5.

2. Governing equations

The dimensionless forced compressible Navier-Stokes equations are

$$\frac{\partial \rho}{\partial t} + \frac{\partial (\rho u_j)}{\partial x_j} = 0 \tag{2.1}$$

$$\frac{\partial (\rho u_i)}{\partial t} + \frac{\partial (\rho u_i u_j)}{\partial x_j} + \frac{\partial p}{\partial x_i} = \frac{1}{Re}\frac{\partial \tau_{ij}}{\partial x_j} + \rho f_i,\ i = 1, \ldots, 3 \tag{2.2}$$

$$\frac{\partial (\rho E)}{\partial t} + \frac{\partial [(\rho E + p) u_j]}{\partial x_j} = \frac{1}{Re}\frac{\partial (u_i \tau_{ij})}{\partial x_j} - \frac{1}{Re\, Pr} C_p \frac{\partial Q_j}{\partial x_j} + \rho W \tag{2.3}$$

$$\frac{\partial (\rho Y_n)}{\partial t} + \frac{\partial (\rho Y_n u_j)}{\partial x_j} = \frac{1}{Re\, Sc_n}\frac{\partial^2 Y_n}{\partial x_j^2} + \rho \omega_n + \rho q_n,\ n = 1, 2. \tag{2.4}$$

Here ρ is the density, $\mathbf{u} = [u_1, u_2, u_3]$ is the velocity vector, p is the pressure, E is the total energy, $\mathbf{Q} = [Q_1, Q_2, Q_3]$ is the heat flux vector given by Fourier's law, C_p being the non-dimensional specific heat at constant pressure. The quantity τ_{ij} is the shear stress tensor, and $Y_n, n = 1, 2$ are scalar fields, Y_1 being the temperature T and Y_2 the vapor mass fraction Y_v, while ω_n are physical source terms for Y_n. In the case of water vapor ($Y_2 = Y_v$), $\omega_2 = \omega_v$ represents the removal of vapor due to condensation. Quantities are made non-dimensional using reference values: ρ_{ref} for the density, a_{ref} for the velocity, p_{ref} for the pressure, l_{ref} for length, T_{ref} for temperature, μ_{ref} for the dynamic viscosity, and $C_{p,\text{ref}}$ for the specific heat. The Reynolds number is defined as $Re = a_{\text{ref}}\, l_{\text{ref}}/(\mu_{\text{ref}}/\rho_{\text{ref}})$. The Schmidt number is defined as $Sc_n = \mu_{\text{ref}}/\rho_{\text{ref}} D_n$, where D_n is the diffusivity of scalar n. For atmospheric conditions vapor diffusivity (given in Pruppacher & Klett 1997, p. 503 is not too different from thermal diffusivity and so we chose $Sc = 0.75$ for both vapor and temperature. Finally, the terms $\rho f_j, \rho W$, ρq_1 , and ρq_2 in (2.2)-(2.4) represent forcing of momentum, total energy, temperature and vapor, respectively and are described in detail in the next section.

The use of compressible equations to simulate atmospheric clouds requires some comment since use of the incompressible or Boussinesq equations is more common. The rms u' of velocity fluctuations in clouds is of the order of 1 to a few meters per second (MacPherson & Isaac 1977). For $u' = 3$ m/s and speed of sound $a = 300$ m/s, the turbulence Mach number $M_t = u'/a = 0.01$. If we were to choose a similar M_t for the simulations, the CFL criterion would lead to a time step that is very small compared with the flow time. Instead we chose $M_t \simeq 0.05$ for the simulations. This leaves the velocity field essentially incompressible, but allows one to run with an affordable time step. However, in weakly

compressible flow, temperature fluctuations are induced by pressure fluctuations and are proportional to M_t^2. Furthermore the mechanisms for temperature fluctuations in the atmosphere are not unrelated to flow induced pressure fluctuations. Thus we have no right to derive the temperature from the energy E which obeys (2.3). For this reason, temperature is obtained independently by solving a scalar transport equation for $Y_1 \equiv T$.

2.1. *Particle treatment*

Due to their small size (less than about ten microns during the condensation phase), the relaxation time $\tau_p = 4\rho_p r^2/18\mu$ of particles is short compared to the smallest turbulence time scale. They can then be treated as tracers which follow the gas according to

$$\frac{d\mathbf{x}_p}{dt} = \mathbf{u}(\mathbf{x}_p, t). \tag{2.5}$$

Gas variables at a particle location $\mathbf{x}_p$ are estimated by linear interpolation, using the values at the nodes of the surrounding cell (see Boivin *et al.* 1998 for details). For the law of droplet growth by condensation we start with equation (15.74) in Seinfeld & Pandis (1997) and ignore the solute contribution to the equilibrium vapor pressure over the drop. We retain the latent heat term as well as the curvature contribution (Kelvin effect) and the kinetic corrections to effective vapor and temperature diffusivities. (We verified *a posteriori* that the last two contributions are negligible for drops $\gtrsim 1\mu$m). We are thus left with

$$\frac{dr}{dt} = \frac{\alpha(r,T)S}{r} \tag{2.6}$$

where $S = Y_v - Y_v^s(T)$ is the local supersaturation with respect to water and $\alpha(r,T)$ is a coefficient that depends on temperature and droplet size. Saturation conditions are obtained from the fit by Sonntag (1994)

$$p_v^s = p\,X_v^s = \exp(\,a_1 \ln T + a_2\,T^{-1} + a_3 + a_4\,T + a_5\,T^2) \tag{2.7}$$

where the mass fraction $Y_v^s(T)$ and molar fraction $X_v^s(T)$ at saturation are related by $Y_v^s = X_v^s/(X_v^s + (1 - X_v^s)\,W_{air}/W_v)$, with $W_{air}/W_v = 28.85/18.01 = 1.6$.

2.2. *Numerical method*

The gas transport equations (2.1)–(2.4) are discretized in physical space by means of the sixth order compact scheme by Lele (1992). They are advanced in time together with (2.5)–(2.6), using a 3rd order Runge-Kutta scheme. Periodic boundary conditions are used in the three directions of the computational cube which has sides $L_{box} = 2\,\pi$. The code is parallelized using domain decomposition with MPI as the communication protocol.

3. Turbulence forcing

In order to obtain a statistically stationary velocity field, a body force $\mathbf{f}(\mathbf{x},t) = [f_1(\mathbf{x},t), f_2(\mathbf{x},t), f_3(\mathbf{x},t)]$ is applied to the momentum equations. Physically, this represents the effect of processes such as turbulence production by shear and the turbulent cascade which occur on scales larger than the computational box. To preserve universality of the smallest scales of turbulence, only the (low) vector-valued wavenumbers $\mathbf{k}$ within the sphere $k \equiv |\mathbf{k}| \leq k_f$ are forced. The force is represented as a finite Fourier

series (see Eswaran & Pope 1988a)

$$\mathbf{f}(\mathbf{x},t) = \sum_{k\le k_f} e^{\mathrm{i}\mathbf{k}\cdot\mathbf{x}}\,\hat{\mathbf{f}}(\mathbf{k},t) \tag{3.1}$$

where $\hat{\mathbf{f}}(\mathbf{k},t) = [\hat{f}_1(\mathbf{k},t), \hat{(}f_2\mathbf{k},t), \hat{f}_3(\mathbf{k},t)]$ and $\hat{f}_j(\mathbf{k},t) \equiv f_j^R(\mathbf{k},t) + \mathrm{i}\, f_j^I(\mathbf{k},t)$ is the Fourier transform corresponding to $\mathbf{k} = k_0\,[l,m,n]$ ($k_0 = 2\pi/L_{box} = 1$ being the fundamental wavenumber), while the summation is intended over the three components, $l = -N/2 + 1,..,N/2$; $m = -N/2+1,..,N/2$; $n = -N/2+1,..,N/2$, with the condition $k = k_0(l^2 + m^2 + n^2)^{1/2} \le k_f$. At each wavenumber, $\hat{\mathbf{f}}(\mathbf{k},t)$ is obtained from the divergence-free projection

$$\hat{\mathbf{f}}(\mathbf{k},t) = \hat{\mathbf{g}}(\mathbf{k},t) - (\mathbf{k}\cdot\hat{\mathbf{g}}(\mathbf{k},t)/k^2)\,\mathbf{k}, \tag{3.2}$$

of the three-dimensional stochastic process $\hat{\mathbf{g}}(\mathbf{k},t) = [\hat{g}_1(\mathbf{k},t), \hat{g}_2(\mathbf{k},t), \hat{g}_3(\mathbf{k},t)]$ which is composed of six independent Uhlenbeck-Ornstein (UO) processes corresponding to the real and imaginary parts of $\hat{g}_j(\mathbf{k},t) = g_j^R(\mathbf{k},t) + \mathrm{i}\, g_j^I(\mathbf{k},t), j = 1,\ldots,3$. These processes are governed by the Langevin stochastic differential equation (Lemons 2002),

$$dg_j^{R,I}(\mathbf{k},t) \equiv g_j^{R,I}(\mathbf{k},t+dt) - g_j^{R,I}(\mathbf{k},t) = -\frac{g_j^{R,I}(\mathbf{k},t)}{\tau_f}\,dt + N_t^{t+dt}(0,1)\sqrt{2\,\sigma_f^2\frac{dt}{\tau_f}} \tag{3.3}$$

where τ_f and σ_f are, respectively, the autocorrelation time and standard deviation of all processes, while $N_t^{t+dt}(0,1)$ is a normally distributed random number with zero mean and unit variance associated with the time interval $[t;t+dt]$. From (3.3) it can be easily shown that each UO process has zero ensemble-mean and is exponentially auto-correlated with time lag τ_f, i.e.

$$\left\langle g_j^{R,I}(\mathbf{k},t)\right\rangle = 0 \tag{3.4}$$

$$\left\langle g_i^{R,I}(\mathbf{k},t)\, g_j^{R,I}(\mathbf{k},t+s)\right\rangle = \sigma_f^2\delta_{ij}^{R,I}e^{-s/\tau_f}. \tag{3.5}$$

Using the condition that f_j be real (i.e. $f_j^R(-\mathbf{k}) = f_j^R(\mathbf{k})$, $f_j^I(-\mathbf{k}) = -f_j^I(\mathbf{k})$) and the requirement $\int_V f_j\,dV = 0$ that the force not change the net linear momentum (i.e. $f_j^R(0) = f_j^I(0) = 0$), one has for the forcing terms f_j and W in (2.2) and (2.3)

$$f_j(\mathbf{x},t) = 2\sum_{l=1}^{N/2}\sum_{m=1}^{N/2}\sum_{n=1}^{N/2}\left[f_j^R(\mathbf{k},t)\cos(\mathbf{k}\cdot\mathbf{x}) - f_j^I(\mathbf{k},t)\sin(\mathbf{k}\cdot\mathbf{x})\right], \quad k\le k_f \tag{3.6}$$

$$W(\mathbf{x},t) = \sum_{j=1}^{3} f_j(\mathbf{x},t)\,u_j(\mathbf{x},t) - \int_V \sum_{j=1}^{3} f_j(\mathbf{y},t)\,u_j(\mathbf{y},t)\,dV(\mathbf{y}). \tag{3.7}$$

The quantity W represents the work done by the force and must be added in compressible flows to maintain consistency between the momentum and energy equations (see e.g. Kida & Orzag 1991). In the statistically stationary state the amount of work done by the forcing equals viscous dissipation to heat. The integral term in (3.7) removes thermal energy in the mean and is necessary to keep the mean internal energy in the computational box from monotonically increasing due to viscous heating.

3.1. *Scalar forcing*

Let us now consider the forcing terms q_n in the scalar equations (2.4), and for the sake of clarity neglect the subscript n which simply identifies the scalar (temperature or

water vapor). The same stochastic forcing as described above is used in (2.4) to drive temperature and vapor fluctuations at the large scales. In actual clouds it is convection and mixing between air parcels, and radiation, etc. that drive the fluctuations. Following the usual approach, one can decompose $q(\mathbf{x},t)$ as

$$q(\mathbf{x},t) = \sum_{k\leq k_f} e^{\mathrm{i}\mathbf{k}\cdot\mathbf{x}}\,\hat{q}(\mathbf{k},t), \quad \text{with} \quad \hat{q}(\mathbf{k},t) \equiv q^R(\mathbf{k},t) + \mathrm{i}\,q^I(\mathbf{k},t), \tag{3.8}$$

where $q^R(\mathbf{k},t)$ and $q^I(\mathbf{k},t)$ are chosen to be UO processes defined by

$$dq^{R,I}(\mathbf{k},t) = -\frac{q^{R,I}(\mathbf{k},t)}{\tau_q}\,dt + N_t^{t+dt}(0,1)\sqrt{2\,\sigma_q^2\frac{dt}{\tau_q}}, \tag{3.9}$$

Using the fact that $q(\mathbf{x},t)$ is real one obtains finally

$$q(\mathbf{x},t) = 2\sum_{l=1}^{N/2}\sum_{m=1}^{N/2}\sum_{n=1}^{N/2}\left[q^R(\mathbf{k},t)\cos(\mathbf{k}\cdot\mathbf{x}) - q^I(\mathbf{k},t)\sin(\mathbf{k}\cdot\mathbf{x})\right], \quad k\leq k_f. \tag{3.10}$$

In (3.9), we chose $\tau_q = \tau_f$ assuming that the same process, namely large eddies, drive scalar and velocity fluctuations. The ampltitude parameter σ_q could be obtained by requiring that the standard deviation of the resulting scalar field (temperature or vapor concentration) be in the range of atmospheric values. Strictly speaking this can only be verified *a posteriori*, however, one can obtain a good prediction of the resulting variance by using the assumption of a particle system, as often done in the simulation of turbulent flows (see Pope 2000). In these kinds of methods, the flow is regarded as an ensemble of fluid particles each carrying a different value for the scalar Y which evolves according to a Langevin equation

$$dY(t) = -\frac{Y(t) - \langle Y\rangle(t)}{\tau_m}\,dt + \sum_{k=1}^{N_f/2}\left[q^R(k,t) + q^I(k,t)\right] \tag{3.11}$$

$$dq^{R,I}(k,t) = -\frac{q^{R,I}(k,t)}{\tau_q}\,dt + N_t^{t+dt}(0,1)\sqrt{2\,\sigma_q^2\frac{dt}{\tau_q}} \tag{3.12}$$

where N_f indicates all forced modes. The first term in (3.11) is a classical exchange-with-the-mean mixing model, τ_m being the mixing time (usually taken to be the integral time scale τ_e of the flow) which is assumed to be equal to forcing time scale, $\tau_m = \tau_f$. From (3.11) one may then derive

$$\frac{d\langle Y\rangle}{dt} = \sum_{k=1}^{N_f/2}\left\langle\left[q^R(k,t) + q^I(k,t)\right]\right\rangle = 0 \tag{3.13}$$

$$\frac{d\,\sigma_Y^2}{dt} = -2\,\frac{\sigma_Y^2}{\tau_m} + 2\sum_{k=1}^{N_f/2}\left\langle Y\left[q^R(k,t) + q^I(k,t)\right]\right\rangle. \tag{3.14}$$

Using (3.4)-(3.5) and (3.9), one finally gets to

$$\langle Y\rangle = \text{const} \equiv \langle Y\rangle_0 \tag{3.15}$$

$$\sigma_Y^2(t) = N_f\frac{\sigma_q^2\tau_e^2}{2}\left(1 - e^{-2t/\tau_e} - \frac{2t}{\tau_e}\,e^{-2\,t/\tau_e} - \frac{t^2}{\tau_e^2}\,e^{-2\,t/\tau_e}\right) \tag{3.16}$$

N	Re	$u' = \sqrt{2/3K}$	L_e/L_{box}	Re_λ	$k_{max}\eta$	$\sigma_{Y_1}/\langle Y_1\rangle$	$\sigma_{Y_2}/\langle Y_2\rangle$
64	2000	0.05	0.162	49	1.15	0.001	0.001
128	3333	0.05	0.162	69	1.68	0.001	0.001

TABLE 1. Flow-field parameters

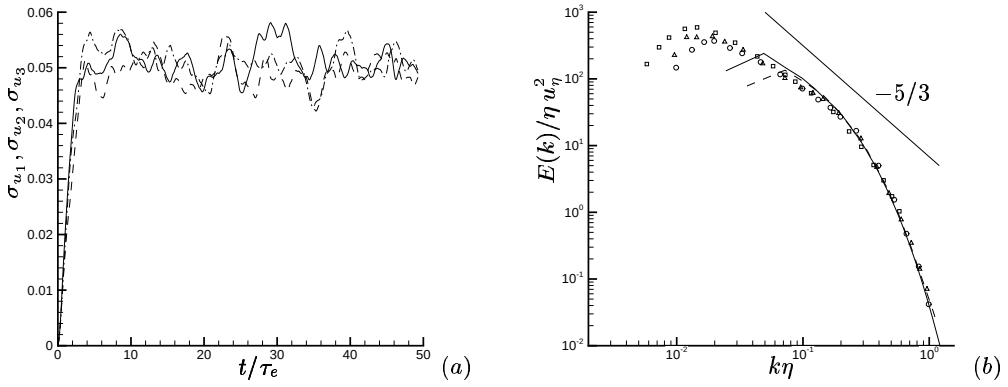

FIGURE 1. (a) Evolution of the standard deviation of the three componets of the velocity field. Particles are introduced at $t/\tau_e = 10$ when the velocity field is statistically stationary. (b) Energy spectra normalized by the Kolmogorov length η and velocity u_η. Solid line: 128^3 simulation; dashed line: 64^3 simulation; symbols: $Re_\lambda \simeq 69$ grid-turbulence experiments of Comte-Bellot & Corrsin (1971).

which shows that σ_Y achieves a stationary value σ_{Y_∞} which satisfies

$$\sigma_q = \frac{\sigma_{Y_\infty}}{\tau_e}\left(\frac{2}{N_f}\right)^{1/2}. \tag{3.17}$$

This relation can be used to design σ_q, knowing some characteristic values for σ_{Y_∞} in the atmosphere. For temperature ($Y \to Y_1 \equiv T$) and vapor concentration ($Y \to Y_2 \equiv Y_v$), Kulmala *et al.* (1997) report $\sigma_{T_\infty} \approx 0.3\,\mathrm{K}$ and $\sigma_{Y_{v\infty}} \approx 1.4 \times 10^{-5}$, which give, for the present simulations, $\sigma_{q_1} = 2.2 \times 10^{-3}$, and $\sigma_{q_2} = 1.0 \times 10^{-6}$. We verified *a posteriori* that these choices did indeed lead to the desired fluctuation levels (see next section).

4. Simulation Results

For each simulation a statistically stationary turbulent flow is first generated according to the method described above. The radius of the sphere of forced wavenumbers is $k_f = \sqrt{8}$, giving a total of $N_f = 92$ forced modes. The standard deviation and autocorrelation time scale of the stochastic forcing were chosen to be, respectively, $\sigma_f = 1.339 \times 10^{-4}$ and $\tau_f = 20.8$ (the same as in Eswaran & Pope 1998b). The resulting turbulence statistics of the flow are provided in Table 1, where $k_{max} \equiv \pi N/L_{box}$, $K = 1/2\,(\sigma_{u_1}^2 + \sigma_{u_2}^2 + \sigma_{u_3}^2)$ is the turbulent kinetic energy, $L_e \equiv L_{11}$ is the longitudinal integral length scale, $Re_\lambda = u'\lambda/\nu$ is the Reynolds number based on the Taylor microscale λ (see Pope 2000 for details). These statitsics were obtained by averaging over samples collected between $t = 10\,\tau_e$,

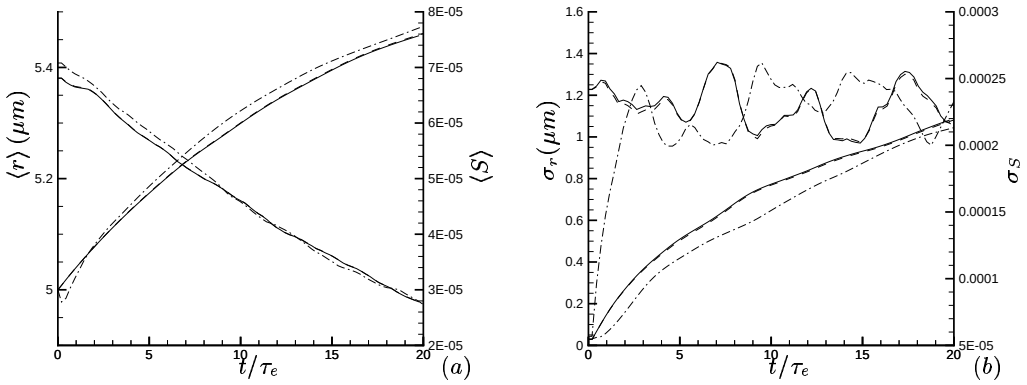

FIGURE 2. Evolution of the statistics of droplet radii r and supersaturation S. (a) Mean values $\langle r\rangle$ and $\langle S\rangle$. The three rising curves show $\langle r\rangle$ while the three falling curves show $\langle S\rangle$. (b) Standard deviations σ_r and σ_S. The three rising curves show σ_r while the three fluctuating curves show σ_S. Line types: ——— , vapor equation is forced throughout (case 1); - - - - , vapor forcing is removed at particle insertion (case 2); —·— , vapor equation is unforced throughout and the vapor field when particles are inserted is set to be random Gaussian (case 3).

when the velocity fluctuations reach their statistically stationary value, up to about $t = 50\,\tau_e$; see Fig. 1a. This figure shows that velocity fluctuations are isotropic; this was also confirmed by examining the two-point longitudinal and transverse correlation functions (not shown). The bulk of the simulations were performed on a 64^3 grid; the rest employed a 128^3 grid which gives a higher Re_λ and allows validation of the method against the grid-turbulence experiments of Comte-Bellot & Corrsin (1971) (see Fig. 1b).

Scalar equations are also forced with the same method, with the means set to $\langle T\rangle = 292K$ and $\langle Y_v\rangle = 0.01415$, respectively. The resulting standard deviations are $\sigma_T \simeq 0.29K$ and $\sigma_{Y_v} \simeq 1.4 \times 10^{-5}$, which are in the range of atmospheric values reported in the literature (see Kulmala *et al.* 1997).

At $t/\tau_e = 50$, $N_p = 96^3$ droplets are randomly distributed in the computational domain and time is then reset to zero. Their number was chosen to satisfy two major constraints: first, it must be high enough that accurate Lagrangian statistics can be obtained, and second, the particle spacing $\lambda = (Vol/N_p)^{1/3}$ must be of the same order of the Kolmogrov scale as in clouds (see Sec. 1). This was indeed verified in the present DNS where $\lambda = 2\pi/96 = 0.67\,\Delta$ or $\lambda = 1.8\,\eta$ (for the 64^3 simulations).

The reference length is taken to be $l_{\rm ref} = 2.5$ cm which implies a dimensional box size of 15.7 cm (for a kinematic viscosty of air $\nu_{\rm ref} = \mu_{\rm ref}/\rho_{\rm ref} = 1.5 \times 10^{-5}\,{\rm m}^2/{\rm s}$, this also sets a reference velocity $a_{\rm ref} = \nu_{\rm ref}\,Re/l_{\rm ref} = 1.2\,{\rm m/s}$, and turbulent fluctuations $\sigma_{u_j} a_{\rm ref} \simeq 6\,{\rm cm/s}$). The droplets are initially monodisperse with radius $r_0 = 5\,\mu$m.

Figure 2 shows the time evolution of the statistics of droplet size and of the local supersaturation. Three cases were run with different types of forcing of the vapor field. Each case is shown using a different line type and is described in the caption. As the mean radius $\langle r\rangle$ increases by condensation, the mean supersaturation $\langle S\rangle$ decreases due to mass conservation. However, their standard deviations are quite different: σ_r increases, up to about $1\,\mu$m while σ_S fluctuates about a certain value. Apart for a short transient in case 3 which is due to the adjustment of water vapor to the turbulent flow, the insensitivity

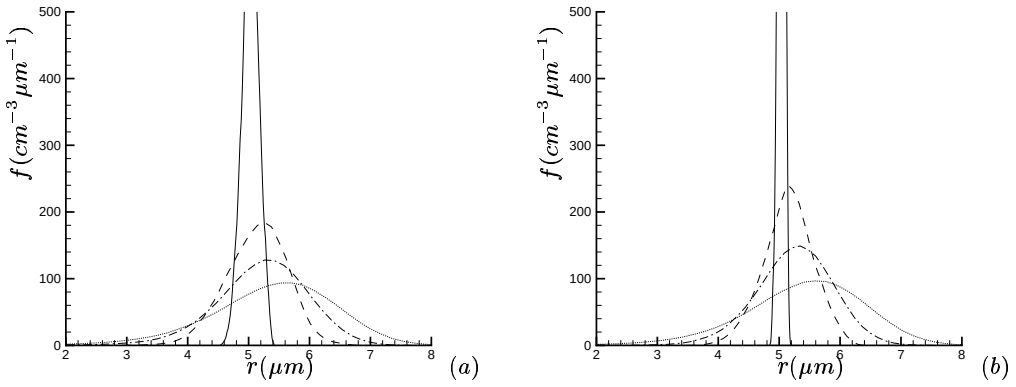

FIGURE 3. Time evolution of droplet size distribution: (a) Case 1; (b) Case 3; ——— , $t = 0.25\,\tau_e$; - - - - , $t = \tau_e$; —·— , $t = 2\,\tau_e$; ····· , $t = 5\,\tau_e$.

of the results to vapor forcing implies that in the present simulations supersaturation fluctuations are mainly controlled by temperature fluctuations.

The increase in σ_r reflects broadening of the droplet size spectrum, as is often observed in cloud measurements (Shaw 2003). This is further shown in Fig. 3 where the distribution of particle radius is plotted at various instants. The mechanism of broadening is that each individual droplet absorbs a fraction of the available supersaturation, depending on the local thermodynamic conditions and water vapor concentration, and grows with its own rate, according to (2.6). Integrating the latter gives

$$r^2(t) = r_0^2 + \int_0^t 2\alpha S(t)\,dt \tag{4.1}$$

which shows that the square of the radius r depends on the time history of supersaturation S. In particular, for two droplets i and j and for a short time t the difference in the radius goes like $r_i^2 - r_j^2 \sim t(S_i - S_j)$. Equation (4.1) also indicates that r and S initially develop a correlation but subsequently turbulent fluctuations decorrelate them. This is clearly shown in Fig. 4 where the correlation coefficient $C_{rS} = \langle r'S' \rangle / \sigma_r \sigma_S$ (S' being evaluated at particle locations) is shown for the two cases with and without forcing the vapor transport equation. The figure shows that, at least for the present Re_λ and dissipation rate, the correlation coefficient is > 0.5 up to $t \equiv \tau_{1/2} = 5\,\tau_e$. It is interesting to compare $\tau_{1/2}$ with the characteristic condensation time for a cloud, which coincides with the supersaturation absorption time (see Khvorostyanov & Curry 1999a), $\tau_f = (4\pi \langle r \rangle_0 D_2 N_p / Vol)^{-1}$. In non-dimensional form, this is $\tau_f = 167 \simeq 8\tau_e$, or $\tau_f \simeq 1.6\,\tau_{1/2}$ for the current simulations. Figure 5 shows scatter plots of r and S at different times for case 1. As the previous figure, they show that $S'/\sigma_S \approx r'/\sigma_r$ up to $t \simeq 2\tau_e$. This result may be used to model the droplet microphysics at the sub-grid scale level in cloud resolving LES, as mentioned e.g. by Paoli & Shariff (2003), and discussed next.

4.1. *Towards a stochastic model of condensation*

One goal of this work was to study the correlation between droplet radius and local supersaturation in a cloud and, eventually, to model it for application in cloud-resolving LES codes. The object of this section is to propose a modeling methodology.

The concept of fluid particles has already been used in Sec. 3 to derive a simple re-

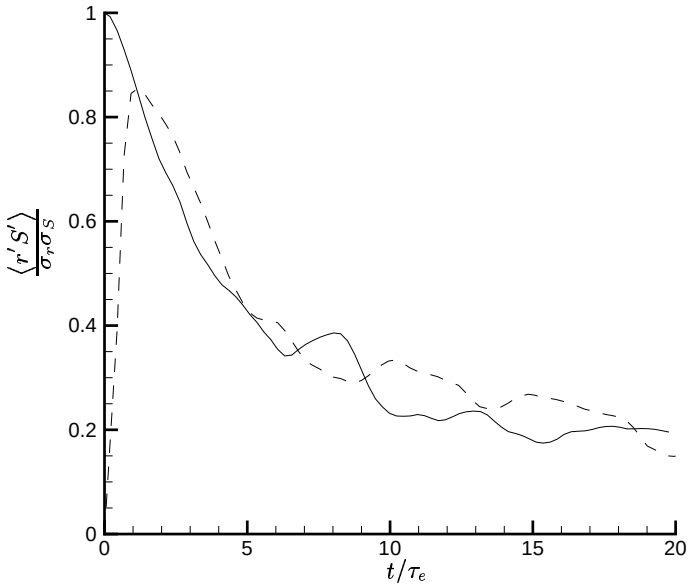

FIGURE 4. Temporal evolution of the radius-supersaturation correlation coefficient: solid line, case 1; dashed line, case 3.

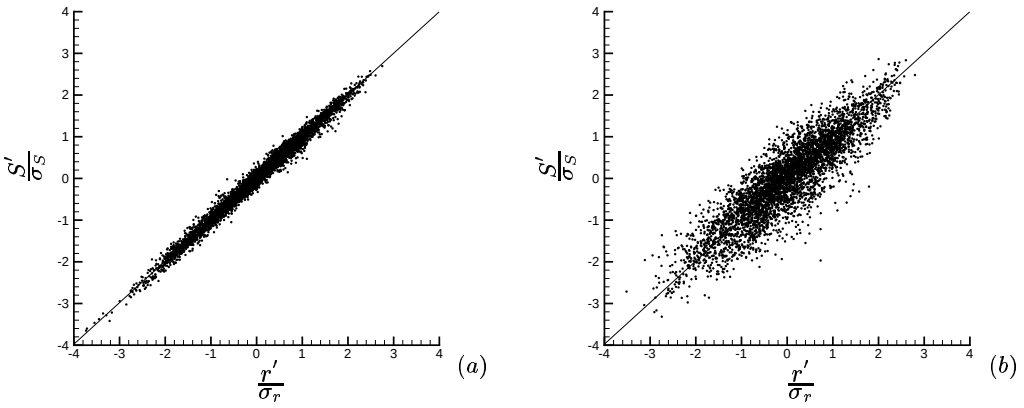

lation between σ_q and σ_{Y_∞}. The same approach is used here for a system of physical droplets, as they have negligible inertia and exactly follow fluid particles. Thus, averaging over droplets is equivalent to volume averaging provided the number of droplets is "sufficiently" high. This has been verified for the present simulations. Assuming a statistically stationary temperature forcing and neglecting water vapor forcing, one can use a Lagrangian formulation to describe temperature and vapor evolution around a physical droplet,

$$dY_v = -\frac{Y_v - \langle Y_v \rangle}{\tau_e}\, dt - 4\pi\alpha\rho_w n_p r^2 \dot{r} \tag{4.2}$$

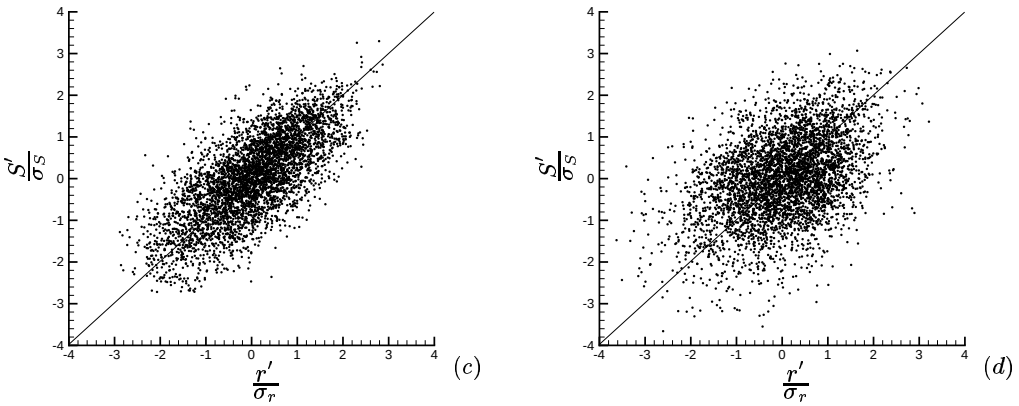

FIGURE 5. Evolution of the scatter plot of droplet radius and supersaturation for case 1 ($r' \equiv r - \langle r \rangle$, $S' \equiv S - \langle S \rangle$): (a) $t = 0.25\,\tau_e$; (b) $t = \tau_e$; (c) $t = 2\,\tau_e$; (d) $t = 5\,\tau_e$.

$$dT = -\frac{T - \langle T \rangle}{\tau_e}\,dt + \sqrt{2\sigma_{T_\infty}^2\,\frac{dt}{\tau_e}}\,N_t^{t+dt}(0,1) \tag{4.3}$$

where n_p is the droplet number density and ρ_w is the water density. Expanding the supersaturation S in (2.7) around the ambient temperature T_∞, one gets after some algebra

$$Y_s(T) \simeq Y_s(T_\infty) + \left(\frac{dY_s}{dT}\right)_{T_\infty}(T - T_\infty) = Y_s(T_\infty)\left[1 + \varphi_\infty (T - T_\infty)\right] \tag{4.4}$$

with $\varphi_\infty = a_1\,T_\infty^{-1} - a_2\,T_\infty^{-2} + a_4 + 2a_5\,T_\infty$. Substituting the latter into Eqs. (4.2) and (4.3) and rewriting for completeness the equation for the growth of droplet radius gives

$$dS = -\frac{S - \langle S \rangle}{\tau_e}\,dt + \varphi_\infty\,Y_s(T_\infty)\sqrt{2\sigma_{T_\infty}^2\,dt} - 4\pi\alpha\rho_w n_p r^2 \dot{r} \tag{4.5}$$

$$dr = \frac{\alpha S}{r}\,dt \tag{4.6}$$

Taking the average of these equations over a population gives

$$\frac{d\langle S \rangle}{dt} = -4\pi\alpha\rho_w n_p \langle S\,r \rangle = -4\pi\alpha\rho_w n_p \left(\langle S \rangle \langle r \rangle + C_{Sr}\,\sigma_r \sigma_S\right) \tag{4.7}$$

$$\frac{d\langle r^2 \rangle}{dt} = \frac{d\langle r \rangle^2}{dt} + \frac{d\langle \sigma_r^2 \rangle}{dt} = 2\alpha \langle S \rangle . \tag{4.8}$$

The problem then is to close, using information from the DNS, the covariances that appear when taking higher moments of r and S (such as, for example, the correlation between r' and S'). This represents the object of our current research.

5. Conclusions

In this brief, a direct numuerical simulation of the turbulent condensation of a population of droplets was perfomed using a coupled Navier-Stokes/Lagrangian code. Forcing of the small wavenumbers was used to sustain velocity, vapor, and temperature fluctuations. The resulting supersaturation fluctuations were responsible for the broadening of

the droplet size distribution in agreement with *in situ* measurements. Finally, a sketch of a possible approach for modeling the correlation between droplet size and supersaturation for use in cloud resolving LES was presented.

Computational resources were provided by the NAS Supercomputing Division at NASA Ames Research Center which is gratefully aknowledged. The first author wishes to thank the Center for Turbulence Research for its hospitality during his post-doctoral stay at NASA Ames and Stanford University.

REFERENCES

Boivin, M., Simonin, O. & Squires, K. D. 1998 Direct numerical simulation of turbulence modulation by particles in isotropic turbulence *J. Fluid Mech.*, **375**, 235–263.

Comte-Bellot, G. & Corrsin, S. 1971 Simple Eulerian time correlation of full and narrow band velocity signals in isotropic turbulence. *J. Fluid Mech.*, **48**, 273–337.

Cooper, W. A. 1989 Effects of variable droplet growth histories on droplet size distributions. Part I: Theory *J. Atmos. Sci.* **46**, 1301–1311.

Eswaran, V. & Pope, S. B. 1988a An examination of forcing in direct numerical simulations of turbulence. *Comput. Fluids*, **16**, 257–278.

Eswaran, V. & Pope, S. B. 1988b Direct numerical simulation of the turbulent mixing of a passive scalar. *Phys. Fluids*, **31**, 506–520.

Khvorostyanov, V. I. & Curry, J. A. 1999*a* Toward the theory of stochastic condensation in clouds. Part I: A general kinetic equation. *J. Atmos. Sci.*, **56**, 3985–3996.

Khvorostyanov, V. I. & Curry, J. A. 1999*b* Toward the theory of stochastic condensation in clouds. Part II: Analytical solutions of the gamma-distribution type *J. Atmos. Sci.*, **56**, 3997-4012.

Kida, S. & Orszag, S. A. 1991 Energy and spectral dynamics in forced compressible turbulence. *J. Sci. Comp.*, **5**, 85–125.

Kulmala, M., Rannik, U., Zapadinsky, E., Clement, C. 1997 The effect of saturation fluctuations on droplet growth. *J. Aerosol Sci.*, **28**, 1395–1409.

Lele, S. K. 1992 Compact finite difference scheme with spectral-like resolution. *J. Comp. Phys.*, **103**, 16–42.

Lemons, D. S. 2002 *An Introduction to Stochastic Processes in Physics.* The Johns Hopkins University Press.

MacPherson, J. I., & Isaac, G. A. 1977 Turbulent characteristics of some Canadian cumulus clouds. *J. Appl. Meteor.*, **16** , 81–90.

Paoli, R., & Shariff, K. 2003 Particle size distributions in atmospheric clouds. *CTR Annual Research Briefs*, 39–47.

Paoli, R., Hélie, J. & Poinsot, T. 2004 Contrail formation in aircraft wakes. *J. Fluid Mech.*, **504** 361–373.

Pinsky, M. B. & Khain, A. P. 1997 Turbulence effects on droplet growth and size distribution in clouds- A review. *J. Aerosol Sci.*, **28**, 1177–1214.

Pope, S. B. 2000 *Turbulent Flows.* Cambridge University Press.

Pruppacher, H. R. & Klett, J. D. 1997 *Microphysics of Clouds and Precipitation.* Kluwer Academic Publishers, Dordrecht, The Netherlands.

SEINFELD, J. N. & PANDIS, S. N. 1997 *Atmospheric Chemistry and Physics: From Air Pollution to Climate Change.* John Wiley & Sons Inc.

SHAW, R. A. 2003 Particle-Turbulence Interactions in Atmospheric Clouds. *Annu. Rev. Fluid Mech.* **35**, 183–227.

SONNTAG, D. 1994 Advancements in the field of hygrometry. *Meteorol. Z.* **3**, 51–66.

SRIVASTAVA, R. C. 1989 Growth of cloud Drops by Condensation: A criticism of currently accepted theory and a new approach. *J. Atmos. Sci.*, **46**, 869–887.

VAILLANCOURT, P. A. & YAU, M. K. 2000 Review of Particle-Turbulence Interactions and Consequences for Cloud Physics. *Bull. Am. Meteorol. Soc.*, **81**, 285–298.